PCCP

Accepted Manuscript

ROYAL SOCIETY OF CHEMISTRY

www.rsc.org/pccp

Cite this: DOI: 10.1039/c0xx00000x

www.rsc.org/pccp

PAPER

Graphene oxide as an anti-shrinkage additive for resorcinol-formaldehyde composite aerogels

Kang Guo, Huaihe Song,* Xiaohong Chen*, Xian Du, Liang Zhong

Received (in XXX, XXX) Xth XXXXXXXXX 20XX, Accepted Xth XXXXXXXXX 20XX

DOI: 10.1039/b000000x

In order to strengthen the nanostructure and suppress the collapse of nanopores of resorcinol-formaldehyde (RF) aerogels in drying process, graphene oxide (GO) was incorporated into RF matrix to prepare GO/RF composite aerogels by sol-gel polymerization. The influences of GO content on the sol-gel process, structure, and physical properties of RF aerogels were investigated. The morphologies of composite aerogels were characterized by scanning electron microscopy and transmission electron microscopy, and it was found that GO was well dispersed in RF matrix. In addition, GO can obviously accelerate the gelation of RF solution and reduce both the drying shrinkage and aerogel density. As the content of GO increased from 0 to 2 wt%, both the linear shrinkage and density of composite aerogels decreased progressively from 28.3% to 2.0% and 506 to 195 $kg \cdot m^{-3}$, respectively, implying that GO is an effective additive for inhibiting the volume shrinkage of aerogels during drying process.

1. Introduction

Resorcinol-formaldehyde (RF) carbon aerogels, as pyrolysis derivatives of RF aerogels, are novel mesoporous carbon materials with many interesting properties, such as low mass densities, continuous porosities, high surface areas, and high electrical conductivities.[1] They are considered to have a wide variety of applications in thermal insulators, electric double layer capacitors, hydrogen fuel storage, and catalyst supports.[2,3] Commonly, carbon aerogels are prepared through the sol–gel polymerization of resorcinol with formaldehyde in aqueous solution, drying of the organic gels, and subsequent high temperature carbonization in an inert gas atmosphere.[4] The great challenge in the preparation of RF aerogels comes from the collapse and shrinkage of nanopores during drying, especially in ambient pressure drying. It was indicated that one of the main reasons for the structural damage of aerogels is the poor mechanical properties of the constituting network.[5,6] Some investigations have been recently explored to strength gel skeletons by adding carbon fibers.[7-9] However, it should be pointed out that the final density of composite simultaneously increases.

Nanocomposite technology using nanoscale fillers at low loading may be an effective way to solve this problem.[10] As a one-dimensional nanostructure material, carbon nanotube (CNT) is considered to be an ideal reinforcing agent for polymer matrix because of its outstanding thermal, electrical, and mechanical properties.[11,12] Recently, graphene oxide (GO) has drawn a great deal of attention as a reinforcing nanofiller in polymer composites due to its low cost,[13] unique two-dimensional honeycomb layer structure,[14] and excellent mechanical property (fracture stress ~ 63 GPa).[15] Compared with CNTs, nanoplatelets have the geometry which can offer isotropic reinforcement in more than one direction, and exhibit more effective reinforcement in polymer composites. Moreover, with numerous oxygen functional groups on surfaces,[16,17] GO can be readily dispersed in water to form stable colloidal suspension and may have strong interfacial bonding with polymer matrix. During the past several years, plenty of polymers, including poly (vinyl alcohol),[18-20] polyurethane,[21] cellulose,[22-24] chitosan,[25,26] phenol-formaldehyde,[27,28] etc., have been used to prepare GO/polymer composites, and their properties, especially the mechanical properties, have been largely enhanced.

Such unique reinforcing behavior of GO attracted our interest to investigate RF aerogels enhanced by GO. Since 2010, several papers on composites of GO and RF aerogels have been published.[29-33] Worsely et al. used RF aerogels as cross-linker in GO suspension (RF:GO=56:44 wt%) to provide conductive interconnections between individual GO sheets.[29] The resulting graphene aerogels displayed high electrical conductivity (87 S/m), which was more than 2 orders of magnitude compared to those for graphene assemblies formed by physical cross-links. Zhang et al. fabricated graphene/RF carbon composite with alkali treated graphene oxide as a base catalyst for the polymerization of R and F, and the composite exhibited excellent rate

State Key Laboratory of Chemical Resource Engineering, Key Laboratory of Carbon Fiber and Functional Polymers, Ministry of Education, Beijing University of Chemical Technology, Beijing, 100029, P.R. China. Fax: +86 10-64434916; Tel: +86 10-64434916; E-mail: songhh@mail.buct.edu.cn chenxh@mail.buct.edu.cn

performance in supercapacitors.[31] However, in these reports, GO was always used in a large amount (~44 wt%), and the effect of GO loading on RF aerogel volume shrinkage has not been studied yet.

In this paper, a small amount of GO was introduced to strengthen gel network and acted as an effective anti-shrinkage nanofiller. We investigated the influences of GO content on the sol-gel process, structure, and physical properties of RF aerogels. It was found that GO can obviously accelerate the gelation of RF solution and reduce both the drying shrinkage and aerogel density. A mechanism of inhibiting shrinkage was proposed.

2. Experimental section

Synthesis of Graphene Oxide

Graphene oxide was synthesized from natural graphite by a modified Hummers method.[34] In a typical process, 5 g of graphite powder was dispersed in 120 ml of concentrated H_2SO_4 with subsequent 2.5 g of sodium nitrate ($NaNO_3$) addition, and the mixture was cooled to 0 °C. Next, 15 g of $KMnO_4$ was slowly added to this mixture, the temperature of which was kept to be below 20 °C by cooling. Stirred at 35 °C for 12 h and then diluted with 600 ml of deionized water, the resultant mixture was then treated by 20 ml H_2O_2 with volume percentage of 30%. After centrifuged at 4000 rpm with 0.1mol/L of HCl aqueous solution (1.5 L) to remove SO_4^{2-}, the obtained yellow mixture was washed with DI water at centrifugal rate of 10000 rpm to remove acid until the mixture became muddy. Then, it was purified by dialysis for one week to remove the remaining metal species and acid. The final GO dispersion was obtained by dilution and sonication with pH of 2.8.

Preparation of GO/RF composite aerogels

GO/RF composite aerogels were prepared by sol-gel polymerizaion of resorcinol (R) and formaldehyde (F) with sodium carbonate as a catalyst (C) in aqueous suspensions containing different concentrations of GO. The molar ratios of R:F and R:C were fixed at 1:2 and 500:1, respectively. The solid concentration of RF solution was controlled at 20 wt%, and the weight content of GO in composite aerogel ranges from 0 to 2 wt% (weight percent of the aerogel, roughly estimated assuming full conversion of R and F into RF aerogel). Sol–gel polymerization of the mixture was carried out in a sealed glass vial (~20 ml) at 20 ℃ for 24 h, then 50 ℃ for 24 h, and finally 90 ℃ for 72 h. The wet gels were immersed in ethanol to remove water from the pores at 40 ℃ for 3 days, and then the resultant gels were completely dried at 40 ℃ under ambient pressure to yield GO/RF aerogels. The GO/RF aerogels with various GO additions were abbreviated as GO/RF-X, where X represents the GO content. For comparison, the RF aerogels were also prepared using the above method without GO.

Characterization

The gelation time was the interval between the introduction of a vial to the water bath at 50 °C and the gelation point (the moment when the sol surface no longer flows at an angle of 45°). The bulk densities of aerogels were calculated from the mass and corresponding volume. The volume was obtained by measuring the dimensions of the monolithic aerogels using Vernier calipers. The linear shrinkage of the resulting aerogels was calculated by the diameter changes of samples before and after drying. Fourier transform infrared spectroscopy (FTIR) spectrum was collected on a Nicolet Nexus 670 spectrometer over the wave range from 4000 to 400 cm^{-1}. Zeta potential measurements were performed using a Zetasizer Nano Series (Malvern) instrument. Aqueous NaOH and HNO_3 solutions were used to adjust the pH. The morphologies and structures of the samples were investigated by scanning electron microscope (SEM, ZEISS SUPRA 55) and transmission electron microscope (TEM, Hitachi H-800). Nitrogen sorption isotherms were measured with ASAP2020 (Micromeritics, USA). The specific surface area and pore size distribution were calculated by the BET (Brunauer–Emmett–Teller) method and BJH (Barrett–Joyner–Halenda) method, respectively.

3. Results and discussion

Characterization of GO

As shown in Fig. 1a, the FTIR spectrum of GO confirms the presence of oxygen-containing groups on GO surface. The bands centered at 1220 and 1620 cm^{-1} are attributed to the deformations of C-O–H groups and the O–H bond in water, respectively.[35,36] The band centered at 1720 cm^{-1} is associated with stretching of the C=O bond of carbonyl or carboxyl groups.[37] Stretching vibration of the C–O bond is observed as the intense band presents at 1060 cm^{-1}.[38] GO aqueous suspension prepared according to the above procedure was stable for several months with no precipitation occurring (inset in the Fig. 1b), and GO can also be suspended in RF solution for a long time. To further study the surface properties of GO, we measured the zeta potential of its aqueous suspension in function of pH (Fig. 1b). We can see that GO sheets are negatively charged in the pH range from 4.0 to 9.0, which is due to the ionization of carboxylic acid and hydroxyl groups existing on the GO sheets. This suggests that electrostatic repulsion between negatively charged GO sheets could generate a stable aqueous suspension.

Gelation Behavior of RF Solution and GO/RF Dispersion

Fig. 2 shows the gelation time of precursor solutions at different GO loadings. The cross-linked network forms much faster in the composite solution than in the pristine solution, and GO/RF-1 shows the shortest gelation time of 93 min, indicating that the introduction of GO into the aerogel system influences the gelation behavior of RF solution. On one hand, the interactions between GO and RF molecules might be existed, and the interactions such as the hydrogen bonding should be responsible for the acceleration of gelation behavior. A similar situation has been reported by Zhang et al, who found that GO can promote the gelation process of cellulose gels and considered that the hydrogen bonding was the reason for the gelation acceleration.[39] On the other hand, since GO is slightly acidic,[40] the pH of precursor solution measured by pH meter monotonously decreases from 6.3 to 5.7 with the GO loading from 0 to 2 wt%. Hyun etc. found that the gelation time was increased with the pH drop of precursor solution.[41] Hence, GO can prolong the gelation time by reducing the pH of precursor

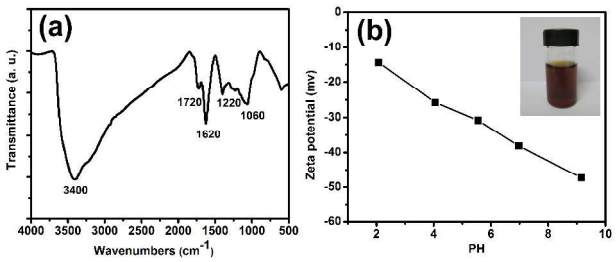

Fig. 1 Surface properties of GO. (a) FTIR transmittance spectra of GO; (b) Zeta potential of GO dispersion in function of pH, and the inset shows the digital picture of GO dispersion at a concentration of 1 mg·ml^{-1}.

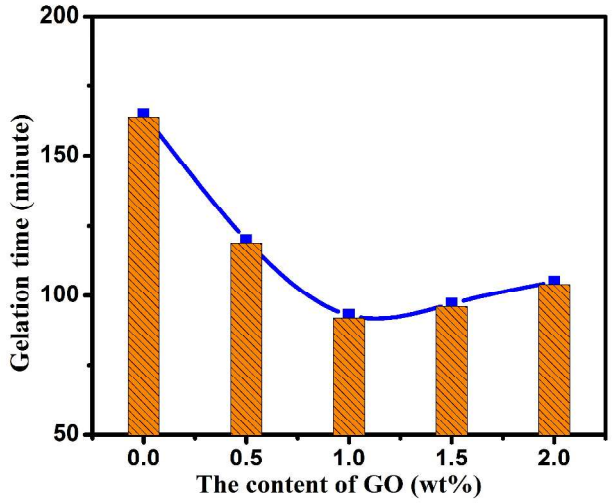

Fig. 2 Gelation time of precursor solutions at different loadings of GO.

solution. Based on the competing effect of the acceleration and prolonging functions, GO can obviously improve the gelation of RF solution and lead to the shortest gelation time with suitable content of 1 %. With more than 1.5 wt% GO, a slight increase in gelation time happened, which may be attributed to the enhancement of the prolonging effect.

Morphologies and structures of RF and GO/RF aerogels

SEM images of RF and GO/RF aerogels with GO loadings ranging from 0 to 2 wt% are shown in Fig. 3. The pristine RF aerogel in Fig. 3a shows smooth and regular surface. As can be seen in Fig. 3c and e, GO is well-dispersed in RF matrix. High magnification SEM images show the interconnected networks of RF nanoparticles, and the size of which increases with GO loading up to 1 wt% (Fig. 3b, d and f). With 2 wt% GO addition, the basic network of GO/RF aerogel changes from nanoparticles to sheets shown in Fig. 3g. Meanwhile, the sizes of RF particles grown on GO surface are mostly larger than 50 nm, and few particles can be observed outside the GO surface (Fig. 3h), indicating that the polymerization of R and F was almost carried out on GO sheets. These could explain the effect of GO on gelation time. With 2 wt% GO, aerogel structure only consists sheets network without nanopariticles network, and thus the

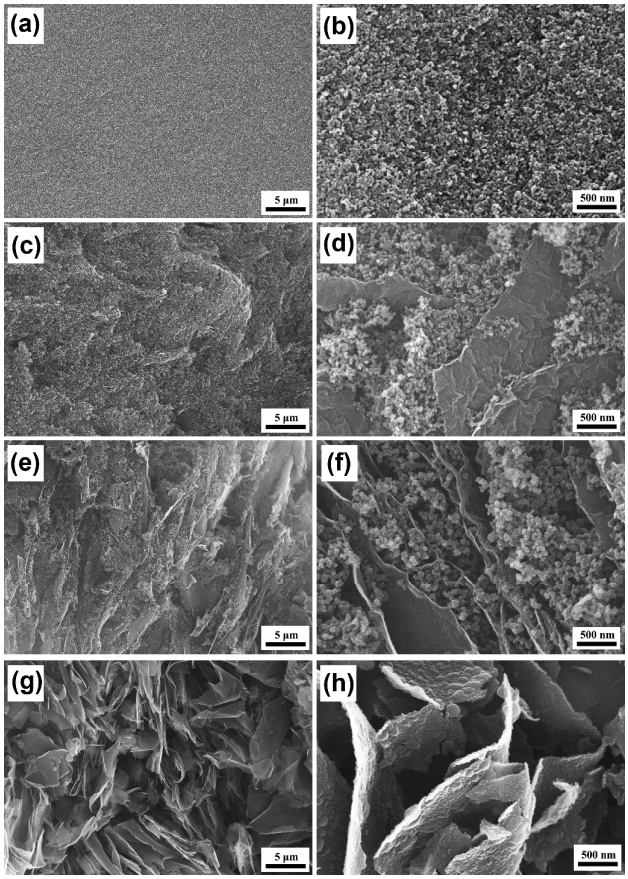

Fig. 3 SEM images of GO/RF composite aerogels with (a, b) pristine RF, (c, d) GO/RF-0.5, (e, f) GO/RF-1, (g, h) GO/RF-2.

prolonging effect in gelation time enhanced, leading to a slight increase in gelation time.

Fig. 4 shows the TEM images of GO/RF-1. As shown in Fig. 4a, a large number of RF particles can be found on the GO surface. This phenomenon can be also found in GO/RF-0.5.These observations suggest good compatibility between GO and RF matrix, which can improve the dispersion and interface interaction of graphene oxide in RF matrix, and further reinforce RF skeleton. In addition, it is interesting to find that RF particles on GO surface (Fig. 4a) with sizes of less than 20 nm are much smaller than those outside the GO surface with sizes of 30-50 nm (Fig. 4b). Pekala and Schaefer pointed out that high catalytic

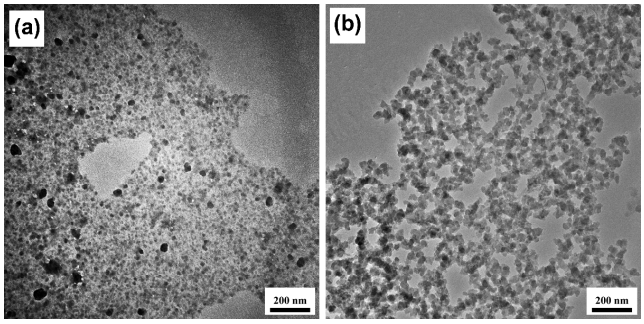

Fig. 4 TEM images of GO/RF-1: (a) on the surface of GO, (b) outside the surface of GO.

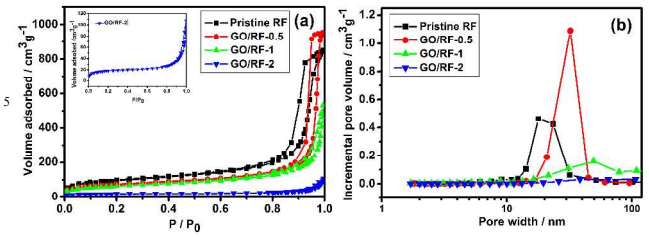

Fig. 5 Nitrogen sorption isotherms (a) and pore size distribution (b) of GO/RF composite aerogels with different GO loadings.

Table 1 Porous attribute of GO/RF composite aerogels

Sample	S_{BET} [a] (m^2g^{-1})	S_{mic} [b] (m^2g^{-1})	S_{mes} [c] (m^2g^{-1})	V_{mes} [d] (cm^3g^{-1})	D_{pore} [e] (nm)
Pristine RF	328	37	291	1.28	17.9
GO/RF-0.5	248	31	217	1.44	32.2
GO/RF-1	223	14	209	0.79	49.4
GO/RF-2	60	18	42	0.15	107.3

[a] BET specific surface area. [b] Microporous surface area. [c] Mesoporous surface area. [d] Mesoporous pore volume. [e] Pore diameter at the peak of the BJH distribution curve.

system can increase the number of resorcinol anions, which can produce highly branched clusters.[42] They are less stable towards spinodal decomposition and thus can lead to smaller particles. Consequently, it can be deduced that, the catalytic activity for the polymerization of R and F is higher on the surface of GO sheets than in the bulk water. A possible mechanism for the polymerization of R and F on GO surface has been supposed. R tends to lose its protons, and the deprotonation of R on the surface of GO sheets will be accelerated because of the presence of negatively charged O^- and COO^- groups on GO. As a result, a large amount of resorcinol anions are produced, leading to smaller RF particles formed on the surface than in the bulk water. If the catalytic activity in bulk water is very low, the RF solution without GO cannot result in gel formation,[43,44] while the RF solution with GO can form a gel. This result indicates the catalytic effect of GO on RF aerogels can expand the scope of RF aerogel formation.

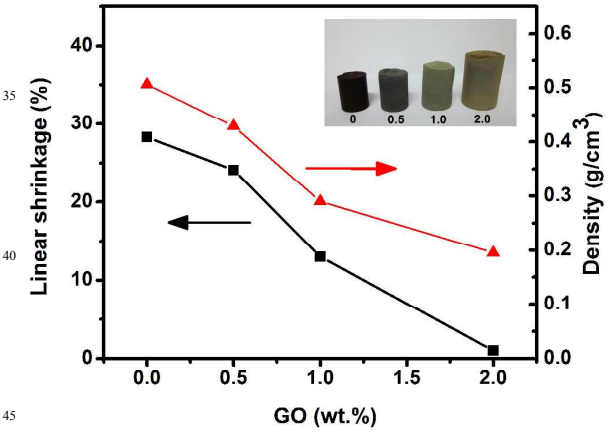

Fig. 6 Linear shrinkage and bulk density of GO/RF composite digital picture of GO/RF composite aerogels. and the inset shows the digital picture of GO/RF composite aerogels.

Fig. 5a shows the N_2 adsorption-desorption isotherms of RF and GO/RF aerogels. Both the pristine RF and GO/RF-0.5 exhibit type IV shape curve according to the IUPAC classification,[44] indicating that the pores of these aerogels are typical mesopores. As the GO loading increases to 1 wt% and 2 wt%, the isotherms are changed into type Ⅱ,[45] consistent with a macroporous adsorbent. Furthermore, substantial specific volumes adsorbed at low P/Po values indicate the presence of micropores. According to the isotherms, surface areas, pore volumes, and pore size distributions of these aerogels were calculated and shown in Table 1 and Fig. 5b. The pores, including mesopores and macropores, in organic aerogels mainly come from the interval gaps between chains of interconnected particles. Due to the increase of RF particle size with GO load, more and more mesopores turn into macropores. Therefore, the centered pore size shifts to larger values, and the pore size distribution becomes broad with increasing GO amount (Fig.5 b). In addition, other porous parameters, such as BET surface area and mesopore surface area, accordingly decrease as shown in Table 1.

Shrinkage and Density of RF and GO/RF aerogels

The effects of GO content on the linear shrinkage and density of GO/RF aerogels during the ambient drying process are shown in Fig.6. The linear shrinkage decreases from 28.3% to 2.0% with GO loadings (0-2 wt%). Simultaneously, the density decreases from 506 to 195 $kg{\cdot}m^{-3}$, and the cause of low densities can be attributed to the decrease in shrinkage of composite aerogel during the ambient drying step. The low density is comparable with that of the RF aerogels obtained by supercritical drying in isopropanol (130 $kg{\cdot}m^{-3}$) [46] and ethanol (260 $kg{\cdot}m^{-3}$) [47]. The macrographs of the GO/RF aerogels at different GO loadings are shown in the inset of Fig. 6. All the samples shown in the inset initially have the same size before ambient drying (near that of the GO/RF-2 on right). The composite aerogels keep monolithic without deformation, which indicates that GO has been well-dispersed in RF matrix, consistent with the observed microstructure in SEM pictures. Moreover, the GO content influenced the optical appearances of RF aerogels drastically. As the GO content arose from 0 to 2 wt%, the color of GO/RF aerogels changed from darkish red to yellowish brown. This can be explained by the fact that GO can decrease the pH of precursor solution and thus reduce the cross-linking degree of RF

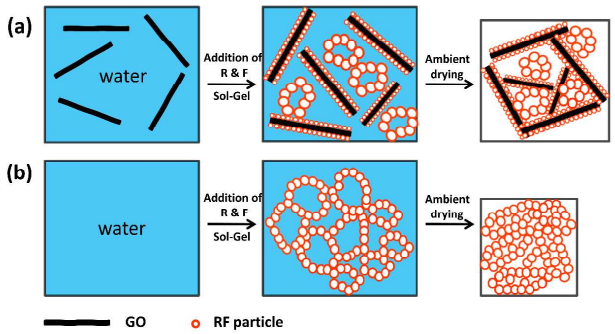

Fig. 7 Schematic diagram of the sol-gel and drying processes of RF solutions with (a) and without GO (b).

aerogels.[48] Fig.7 gives a schematic diagram for the sol-gel and drying processes with GO addition. Ascribed to the strong capillary force on solid framework and the poor mechanical properties of fractal network, pristine RF wet gels had serious collapse and shrinkage during the ambient pressure drying. However, the composite wet gels with GO shrink much less than the pristine ones. Three factors can be taken into account to explain the significant decrease in aerogel shrinkage: (i) According to the excellent mechanical strength and dispersibility, as well as the strong interaction with the RF matrix, GO can significantly reinforce the network of gels and improve the resistance to collapse during drying process; (ii) GO can decrease the pH of precursor solution, leading to the pore size increase and the capillary pressure reduction inside the matrix of aerogels; (iii) Acting as huge barriers between RF nanoparticles, GO can obviously prevent the connection of particles, which may reduce the collapse of gels.

Conclusions

We have prepared RF composite aerogels with graphene oxide as an anti-shrinkage additive by a simple sol-gel polymerization method. Morphological studies showed that GO can be well-dispersed in RF matrix owing to the good compatibility between the two elements, which effectively strengthen the RF skeleton. GO can obviously accelerate the gelation of RF solution and reduce both the drying shrinkage and aerogel density. The linear shrinkage decreases progressively from 28.3% to 2.0 % with GO loadings (0-2 wt%); simultaneously, the density decreases from 506 to 195 kg·m^{-3}. This work offers a new method for the inhibition of aerogel shrinkage and also broadens the application scope of GO.

Acknowledgements

This work was supported by the National Natural Science Foundation of China (51202009 and 51272016), New Teachers' Fund for Doctor Stations, Ministry of Education of China (20120010120004), and Foundation of Excellent Doctoral Dissertation of Beijing City (YB20121001001)

Notes and references

1 S. A. Al-Muhtaseb and J. A. Ritter, *Adv. Mater.*, 2003, **15**, 101.
2 X. Lu, M. Arduini-Schuster, J. Kuhn, O. Nilsson, J. Fricke and R. Pekala, *Science*, 1992, **255**, 971.
3 J. Biener, M. Stadermann, M. Suss, M. A. Worsley, M. M. Biener, K. A. Rose and T. F. Baumann, *Energy Environ. Sci.*, 2011, **4**, 656.
4 R. Pekala, *J. Mater. Sci.*, 1989, **24**, 3221.
5 N. Job, A. Théry, R. Pirard, J. Marien, L. Kocon, J.-N. Rouzaud, F. Béguin and J.-P. Pirard, Carbon, 2005, **43**, 2481.
6 N. Hüsing and U. Schubert, *Angew. Chem. Int. Ed.*, 1998, **37**, 22.
7 R. Fu, B. Zheng, J. Liu, S. Weiss, J. Y. Ying, M. S. Dresselhaus, G. Dresselhaus, J. H. Satcher and T. F. Baumann, *J. Mater. Res*., 2003, **18**, 2765.
8 V. Drach, M. Wiener, G. Reichenauer, H.-P. Ebert and J. Fricke, *Int. J. Thermophy.*, 2007, **28**, 1542.
9 J. Feng, C. Zhang, J. Feng, Y. Jiang and N. Zhao, *ACS Appl. Mater. Inter.*, 2011, **3**, 4796.
10 J. Liang, Y. Huang, L. Zhang, Y. Wang, Y. Ma, T. Guo and Y. Chen, *Adv. Funct. Mater.*, 2009, **19**, 2297.
11 V. N. Popov, *Mater. Sci. Eng. R*, 2004, **43**, 61.
12 H. Qian, E. S. Greenhalgh, M. S. Shaffer and A. Bismarck, *J. Mater. Chem.*, 2010, **20**, 4751.
13 D. A. Dikin, S. Stankovich, E. J. Zimney, R. D. Piner, G. H. Dommett, G. Evmenenko, S. T. Nguyen and R. S. Ruoff, *Nature*, 2007, **448**, 457.
14 O. C. Compton and S. T. Nguyen, *Small*, 2010, **6**, 711.
15 P. Podsiadlo, A. K. Kaushik, E. M. Arruda, A. M. Waas, B. S. Shim, J. Xu, H. Nandivada, B. G. Pumplin, J. Lahann and A. Ramamoorthy, *Science*, 2007, **318**, 80.
16 S. Stankovich, D. A. Dikin, R. D. Piner, K. A. Kohlhaas, A. Kleinhammes, Y. Jia, Y. Wu, S. T. Nguyen and R. S. Ruoff, *Carbon*, 2007, **45**, 1558.
17 H. C. Schniepp, J.-L. Li, M. J. McAllister, H. Sai, M. Herrera-Alonso, D. H. Adamson, R. K. Prud'homme, R. Car, D. A. Saville and I. A. Aksay, *J. Phys. Chem. B*, 2006, **110**, 8535.
18 Y. Xu, W. Hong, H. Bai, C. Li and G. Shi, *Carbon*, 2009, **47**, 3538.
19 X. Yang, S. Shang and L. Li, *J. Appl. Polym. Sci.*, 2011, **120**, 1355.
20 L. Zhang, Z. Wang, C. Xu, Y. Li, J. Gao, W. Wang and Y. Liu, *J. Mate. Chem.*, 2011, **21**, 10399.
21 X. Wang, Y. Hu, L. Song, H. Yang, W. Xing and H. Lu, *J. Mater. Chem.*, 2011, **21**, 4222.
22 N. D. Luong, N. Pahimanolis, U. Hippi, J. T. Korhonen, J. Ruokolainen, L.-S. Johansson, J.-D. Nam and J. Seppälä, *J. Mater. Chem.*, 2011, **21**, 13991.
23 J. Zhang, Y. Cao, J. Feng and P. Wu, *J. Phys. Chem. C*, 2012, **116**, 8063.
24 B. Wang, W. Lou, X. Wang and J. Hao, *J. Mater. Chem.*, 2012, **22**, 12859.
25 X. Yang, Y. Tu, L. Li, S. Shang and X.-m. Tao, *ACS Appl. Mater. Inter.*, 2010, **2**, 1707.
26 H. Fan, L. Wang, K. Zhao, N. Li, Z. Shi, Z. Ge and Z. Jin, *Biomacromolecules*, 2010, **11**, 2345.
27 L. Liu, J. Yang and Q. Meng, *J. Sol-Gel Sci. Technol.*, 2013, **66**, 1.
28 L. Liu, J. Yang and Q. Meng, *J. Sol-Gel Sci. Technol.*, 2013, **67**, 304.
29 M. A. Worsley, P. J. Pauzauskie, T. Y. Olson, J. Biener, J. H. Satcher Jr and T. F. Baumann, *J. Am. Chem. Soc.*, 2010, **132**, 14067.
30 M. A. Worsley, T. Y. Olson, J. R. Lee, T. M. Willey, M. H. Nielsen, S. K. Roberts, P. J. Pauzauskie, J. Biener, J. H. Satcher Jr and T. F. Baumann, *J. Phy. Chem. Lett.*, 2011, **2**, 921.
31 F. Meng, X. Zhang, B. Xu, S. Yue, H. Guo and Y. Luo, *J. Mater. Chem.*, 2011, **21**, 18537.
32 K. Zhang, B. T. Ang, L. L. Zhang, X. S. Zhao and J. Wu, *J. Mater. Chem.*, 2011, **21**, 2663.
33 Y. J. Lee, H. W. Park, G.-P. Kim, J. Yi and I. K. Song, *Curr. Appl. Phys.*, 2013, **13**, 945.
34 W. S. Hummers Jr and R. E. Offeman, *J. Am. Chem. Soc.*, 1958, **80**, 1339.
35 D. C. Marcano, D. V. Kosynkin, J. M. Berlin, A. Sinitskii, Z. Sun, A. Slesarev, L. B. Alemany, W. Lu and J. M. Tour, *ACS nano*, 2010, **4**, 4806.
36 C. Hontoria-Lucas, A. Lopez-Peinado, J. d. D. López-González, M. Rojas-Cervantes and R. Martin-Aranda, *Carbon*, 1995, **33**, 1585.
37 J. Paredes, S. Villar-Rodil, A. Martinez-Alonso and J. Tascon, *Langmuir*, 2008, **24**, 10560.
38 Y. Xu, H. Bai, G. Lu, C. Li and G. Shi, *J. Am. Chem. Soc.*, 2008, **130**, 5856.
39 J Zhang, Y Cao, J Feng and P Wu, *J. Phy. Chem. C*, 2012, 116, 8063.
40 T. Szabó, E. Tombácz, E. Illés and I. Dékány, *Carbon*, 2006, **44**, 537.
41 S.-W. Hwang and S.-H. Hyun, *J. Non-Cryst. Solids*, 2004, **347**, 238.
42 R. Pekala and D. Schaefer, *Macromolecules*, 1993, **26**, 5487.
43 V. Bock, A. Emmerling, R. Saliger and J. Fricke, *J. Porous Mater.*, 1997, **4**, 287.
44 C. Lin and J. Ritter, *Carbon*, 1997, **35**, 1271.
45 K. Sing, K. Sing, D. Everett, R. Haul, L. Moscou, R. Pierotti, J. Rouquerol and T. Siemieniewska, *Pure Appl. Chem.*, 1982, **54**, 2201.
46 R. Fu, B. Zheng, J. Liu, M. S. Dresselhaus, G. Dresselhaus, J. H. Satcher and T. F. Baumann, *Adv. Funct. Mater.*, 2003, **13**, 558.
47 D. Wu, R. Fu and Z. Yu, *J. Appl. Polym. Sci.*, 2005, **96**, 1429.
48 A. M. ElKhatat and S. A. Al-Muhtaseb, *Adv. Mater.*, 2011, **23**, 2887.